ACS OMEGA

Open Access

http://pubs.acs.org/journal/acsodf

Article

Silk Industry Waste Protein-Derived Sericin Hybrid Nanoflowers for Antibiotics Remediation via Circular Economy

Divya S. Koshy, Benjamin J. Allardyce, Ludovic F. Dumée, Alessandra Sutti, Rangam Rajkhowa, and Ruchi Agrawal*

Cite This: *ACS Omega* 2024, 9, 15768−15780

Read Online

ACCESS | Metrics & More | Article Recommendations | Supporting Information

ABSTRACT: Hybrid protein−copper nanoflowers have emerged as promising materials with diverse applications in biocatalysis, biosensing, and bioremediation. Sericin, a waste biopolymer from the textile industry, has shown potential for fabricating such nanoflowers. However, the influence of the molecular weight of sericin on nanoflower morphology and peroxidase-like activity remains unexplored. This work focused on the self-assembly of nanoflowers using high- and low-molecular-weight (HMW and LMW) silk sericin combined with copper(II) as an inorganic moiety. The peroxidase-like activity of the resulting nanoflowers was evaluated using 2,2′-azino-bis(3-ethylbenzothiazoline-6-sulfonic acid) (ABTS) and hydrogen peroxide (H_2O_2). The findings revealed that high-molecular-weight sericin hybrid nanoflowers (HMW-ShNFs) exhibited significantly higher peroxidase-like activity than low-molecular-weight sericin hybrid nanoflowers (LMW-ShNFs). Furthermore, HMW-ShNFs demonstrated superior reusability and storage stability, thereby enhancing their potential for practical use. This study also explored the application of HMW-ShNF for ciprofloxacin degradation to address the environmental and health hazards posed by this antibiotic in water. The results indicated that HMW-ShNFs facilitated the degradation of ciprofloxacin, achieving a maximum degradation of 33.2 ± 1% at pH 8 and 35 °C after 72 h. Overall, the enhanced peroxidase-like activity and successful application in ciprofloxacin degradation underscore the potential of HMW-ShNFs for a sustainable and ecofriendly remediation process. These findings open avenues for the further exploration and utilization of hybrid nanoflowers in various environmental applications.

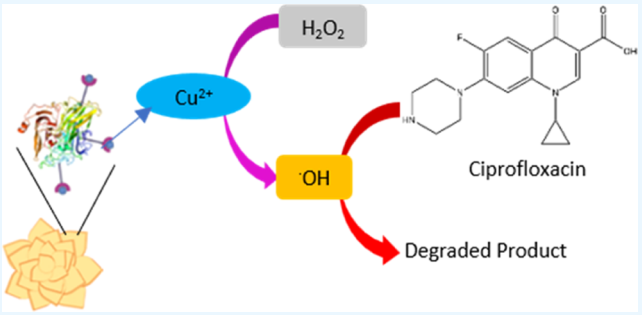

1. INTRODUCTION

The past decade has witnessed an increased focus on hybrid protein−inorganic nanoflowers (hNFs) for various applications, such as biosensing,[1−9] drug delivery,[10] adsorption,[11] biocatalysis,[12−16] and wastewater treatment.[16−22] Typically, hybrid nanoflowers are highly porous nanostructured materials with a high surface area. They form via the complexation of metal phosphates with nitrogen- and oxygen-rich groups present in the protein components, such as amide and amine groups,[23] ketone groups,[24] carboxyl and diol groups.[25] Most hNFs are considered to be nontoxic and biocompatible, with enhanced stability and improved efficacy of surface reactions.[26,27] The mechanism of the formation of hybrid nanoflowers has been investigated in depth.[23,28] The aggregation of proteins leads to partial crystallization, whereby metal phosphate crystals are formed at discrete metal ion binding sites on the surface of agglomerates, inducing discrete petals to grow.[29,30] The complexation of metal ions by protein molecules plays a critical role in enhancing the functionalities of these hybrid materials. Hybrid nanoflowers have good stability, durability, and activity.[7,11,17,23,31,32] The impact of factors like the concentration, nature of proteins/enzymes, metal ions, pH, time, and temperature are frequently explored. To the best of our knowledge, however, the influence of the molecular weight of the proteins/enzymes on morphology, activity, stability, and reusability has not been often explored.

Silkworm sericin, a gum-like protein that acts as a glue to hold the cocoon together,[33−35] is a useful protein for the formation of nanoflowers because it is a widely available waste from the silk textile industry.[36] Sericin is also biocompatible, biodegradable, sustainable, and has antioxidant properties.[37] The high content of polar functional groups with lone electron pairs in sericin molecules provides a high likelihood of coordination of some protein groups with metal ions with electron-deficient d-orbitals.[38] Previously, sericin nanoflowers have been reported for the removal of heavy metals like Hg, Cd, and Pb as well as Congo red.[11,39] In a few recent studies,

Received: May 15, 2023
Revised: February 13, 2024
Accepted: February 14, 2024
Published: March 25, 2024

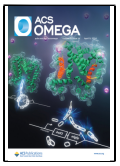

nanoflowers incorporating amino acids,[40] catecholamines,[41] β-lactoglobulin, and α-lactalbumin[42] have been studied for their peroxidase-like activity, which opens a new opportunity for sustainable and affordable biocatalysts. However, the use of sericin hybrid nanoflowers (ShNFs) as biocatalysts for peroxidase-like activity has not yet been explored. Since sericin is dumped as a waste product in tons from the textile industry, finding suitable extraction techniques for the preparation of nanoflowers will not only help in reducing water pollution but also be economically beneficial. Thus, the current study is a "circular economy" approach to utilize waste sericin protein for high-value bioproducts.

One potential application of nanoflowers is the degradation of active pharmaceutical compounds, such as antibiotics released into the water. Ciprofloxacin (CIPRO) is a broad-spectrum antibiotic used for the treatment of humans and animals, and is found in concerning levels in drinking water and other natural sources of water, leading to detrimental effects on the ecosystem and human health. According to the US FDA, concentrations above 1 μg/L are considered to be toxic.[43,44] Larsson et al.[44] reported a very high concentration of ciprofloxacin (31,000 μg/L) and the development of antibiotic-resistant pathogens in India. Balakrishna et al.[45] reported a 40 times higher concentration of ciprofloxacin in Indian water systems compared to other countries. Sengar and Vijayanandan[46] reported a significantly high-risk quotient (RQ) for ciprofloxacin among 98 pharmaceuticals. To address the inefficacy of conventional water treatment technologies for the removal of ciprofloxacin and its metabolites, various technologies, such as advanced oxidation processes, photodegradation, electrochemical processes, adsorption, and biodegradation[47−49] have been reported. In particular, biodegradation has drawn a lot of attention because of its affordability, effectiveness, and environmental-friendliness.[50−52]

In this study, two different types of sericin hybrid nanoflowers (ShNFs) were synthesized with chemically extracted high- and low-molecular-weight (HMW and LMW) sericin as the organic component and copper(II) as the metal ion counterpart. The variation in the morphology of sericin nanoflowers as a function of the molecular weight of sericin and the concentrations of sericin and copper(II) were explored. The peroxidase-like activity of sericin hybrid nanoflowers was investigated using ABTS and H_2O_2. Further, for the first time, the peroxidase-like activity of sericin hybrid nanoflowers was used for the degradation of ciprofloxacin.

2. MATERIALS AND METHODS

2.1. Chemicals and Materials. Bivoltine *Bombyx mori* reeled fibers were purchased from an automatic silk reeling unit (Ramanagaram, India). Ciprofloxacin (catalog no. 17850) from Sigma-Aldrich (Israel) and 2,2′-azino-bis(3-ethylbenzothiazoline-6-sulfonic acid) (ABTS) (catalog no. A1888) from Sigma-Aldrich were used as procured. Copper sulfate pentahydrate was procured from Merck. 30% hydrogen peroxide was procured from Analytical Reagents (CDH) (India). Guanidine hydrochloride and sodium carbonate were obtained from Sigma, and sodium chloride and potassium dihydrogen orthophosphate were obtained from Qualigens (India). Potassium chloride and disodium hydrogen orthophosphate were procured from Fisher Scientific. NuPAGE 3−8% Tris-acetate gel, Colloidal Blue staining kit, HiMark Unstained Protein Standard, and the Novex Sharp Prestained Protein Standard were procured from ThermoFisher. Acetic acid from Merck, and sodium acetate anhydrous from Himedia (India) were used for the preparation of buffers. Hydrochloric acid and sodium hydroxide were used to adjust the pH of the buffers. All chemicals used were of 98−99% purity.

2.2. Extraction of Sericin and Molecular Weight Determination by Sodium Dodecyl Sulfate-Polyacrylamide Gel Electrophoresis (SDS-PAGE). Undegummed reeled bivoltine silk fibers were cleaned and cut into small fragments of similar sizes. Sericin was extracted by using two different chemical approaches.

The first approach employed 6 M guanidine hydrochloride (GuHCl) for removing sericin. Cut fibers (3 g) were immersed in 30 mL of a GuHCl solution (1:10 ratio) at 60 °C for 1 h. To recover sericin, the solution was dialyzed for 24−48 h using 10 kDa dialysis membranes.

In the second approach, the silk fibers were immersed in 0.02 M sodium carbonate in a 1:30 ratio at 100 °C for 1 h. The extraction of sericin from *Bombyx mori* cocoons using sodium carbonate is the most used technique in the textile industry.[53] To recover sericin, the solution was dialyzed for 3 days against deionized (DI) water, using 10 kDa dialysis membranes.[54]

The molecular weight of sericin extracted using both approaches was determined using sodium dodecyl sulfate-polyacrylamide gel electrophoresis (SDS-PAGE) following the Laemmli[55] method. Briefly, an aliquot containing 30 μg of each sericin sample was loaded into the wells of a NuPAGE 3−8% Tris-acetate gel and run alongside two protein standards: the HiMark Unstained Protein Standard and the Novex Sharp Prestained Protein Standard. Electrophoresis was carried out at 150 V for 1 h at a constant voltage. The gels were stained using a Colloidal Blue staining kit and photographed with a Gel Doc XRS+ Gel Documentation System (Bio-Rad, Hercules, CA).

2.3. Synthesis of Sericin Hybrid Nanoflowers (ShNFs). Nanoflowers were prepared as previously reported by Ge et al.[23] with slight modifications. 83.3 μL of aqueous 120 mM copper sulfate pentahydrate ($CuSO_4{\cdot}5H_2O$) solution was added to 10 mL of phosphate-buffered saline (PBS, 10 mM, pH 7.4) containing 0.1 mg/mL HMW sericin or LMW sericin to obtain a final concentration of copper(II) of 1 mM. The mixture was vortexed thoroughly and incubated at room temperature (RT) for 72 h without any disturbance. After incubation, the nanoflowers were separated from the supernatant by centrifugation at 4000 RCF for 10 min and washed with DI water 3−4 times to remove any unreacted components. The nanoflowers were air-dried overnight. The effects of sericin concentration (0.02−0.1 mg/mL) and copper(II) concentration (0.6−1.0 mM) were also studied. The control copper phosphate trihydrate [$Cu_3(PO_4)_2{\cdot}3H_2O$] precipitates were prepared by the addition of a 120 mM $CuSO_4{\cdot}5H_2O$ solution in PBS without sericin.

2.4. Characterization of ShNFs. Morphological characterization of the ShNFs was carried out using a field emission scanning electron microscope (SEM, Zeiss SUPRA 55VP, Germany). The working distance was set to 10.5 mm with an accelerating voltage of 10 kV. Energy dispersive X-ray (EDX) spectroscopy was performed using an LN2 detector (EDAX Inc., Netherlands).

To estimate the protein loading efficacy in the nanoflowers, the bicinchoninic acid (BCA) assay was used with bovine serum albumin (BSA) as the standard. The absorbance of the purple-colored soluble complex was measured at 562 nm. The protein loading was calculated by using the following formula:

https://doi.org/10.1021/acsomega.3c03367
ACS Omega 2024, 9, 15768−15780

$$E\% = \frac{(A^0 - A)}{A^0} \times 100 \quad (1)$$

where A^0 and A are the initial and final concentrations of sericin, respectively. A Synergy H1 Hybrid Microplate reader (Biotek Life Science Instrumentation) was used for recording absorbance.

Fourier transform infrared (FTIR) spectroscopy was performed using a Bruker Vertex 70 FTIR (4000−600 cm^{-1}). The number of scans was 64, and the scanning rate was 2 cm^{-1}/min.

X-ray diffraction (XRD) analysis was done on a PANalytical X'Pert Pro MPD diffractometer (Netherlands). The 2θ scanning range was 5−70° at 0.013° intervals with Cu Kα radiation (λ = 1.5406 Å and 40 kV/30 mA).

2.5. Peroxidase-Like Activity of ShNFs. The peroxidase-like activities of different ShNFs and $Cu_3(PO_4)_2{\cdot}3H_2O$ precipitates were estimated as described by Wu et al.[40] with slight modifications using 100 mM sodium acetate at pH 4.5, 1.5 mM ABTS, and 8 mM H_2O_2. For the assay, ShNFs (1 mg of dry mass) were suspended in 1 mL of buffer to prepare a 1 mg/mL stock solution. The mixture was vortexed until it became homogeneous. Next, 300 μL of ABTS and 300 μL of H_2O_2 were added to 300 μL of this mixture. The reaction mixture was thoroughly vortexed and incubated for 30 min at 35 °C in a water bath. Following incubation, the evolution of the green-colored supernatant formed by the radical cation $ABTS^{\bullet+}$ was quantified by measuring the light absorbance at 417 nm. One unit of peroxidase activity was defined as the amount of the biomimetic catalyst that catalyzes the conversion of 1 nmol of ABTS per minute under standard conditions.[56]

2.6. Reusability and Stability Test of ShNFs. The reusability assessment of the peroxidase-like activity of the ShNFs was performed, as described in Section 2.5. After each cycle, the nanoflowers were separated from the reaction medium by centrifugation at 4000 RCF for 5 min, washed thoroughly with deionized (DI) water three times, and resuspended in a working buffer.[57]

The storage stability of the ShNFs was also evaluated, wherein the ShNFs were stored in PBS at 4 °C for 30 days, and peroxidase-like activity was determined every seventh day. Also, the nanoflowers were subjected to SEM imaging after the determination of peroxidase activity.

2.7. Kinetics of Peroxidase Activity of ShNFs. The kinetics of the peroxidase activity of both HMW-ShNFs and LMW-ShNFs were measured, as described by Wang et al.[58] with some modifications by varying the ABTS concentrations from 0.1 to 5 mM and keeping the concentration of H_2O_2 constant at 8 mM. 80 μL of H_2O_2 was added to varying volumes of ABTS and ShNFs (1 mg/mL), followed by incubation at 35 °C in a water bath for 10 min. Then, the mixture was mixed thoroughly and again incubated at 35 °C. The absorbance at 417 nm was measured every 30 s for 30 min using a Synergy1 Hybrid Microplate Reader. The graphs were plotted by using the GraphPad Prism 8.0.2 software package. The kinetic parameters K_m and V_{max} were determined by plotting the initial rate of reaction against the substrate concentration using the Michaelis−Menten curve. K_m is the Michaelis−Menten constant, which indicates the concentration of the substrate when the rate of the reaction is half of the maximum rate of reaction and V_{max} is the maximum rate of reaction. Nonlinear regression was used to obtain the kinetic parameters using the software GraphPad Prism 8.0.2.

2.8. Peroxidase-Based Study of Ciprofloxacin (CIPRO) Degradation Using HMW-ShNFs. HMW-ShNFs (1 mg) were suspended in 1 mL of ciprofloxacin (10 ppm) prepared in a working buffer. The vial was kept at 35 °C and 1000 rpm in a thermomixer for 30 min in the dark to attain equilibrium. The required amount of H_2O_2 (30%) was then added to the reaction mixture. After 24 h, the reaction mixtures were centrifuged at 4000 RCF for 10 min, and 100 μL of sodium thiosulfate (10 mM) was added to the supernatant to quench the hydroxyl radicals ($OH^{\bullet}$), which were then quantified for residual CIPRO. For quantitative analysis of ciprofloxacin, a UV−visible spectrophotometer (Shimadzu (Asia Pacific) Pvt Ltd.) was used. The residual concentration of ciprofloxacin was derived by using the absorption values at 278 nm from the standard curve prepared. The percentage degradation was calculated using the following equation:

$$d\% = \frac{(C_0 - C_t)}{C_0} \times 100 \quad (2)$$

where d% is the degradation efficiency, and C_0 and C_t are the concentrations at the beginning and at time t of degradation, respectively. The effect of the pH of the working buffer, the concentration of H_2O_2, the concentration of HMW-ShNFs, and time were evaluated in this study.

2.9. Statistical Analysis. All experiments were conducted in triplicate, and all results are reported as mean ± standard deviation. The average size of the nanoflowers was determined by measuring 50−100 nanoflowers using ImageJ. GraphPad Prism version 8 was used to plot all of the graphs. A significant difference ($p < 0.05$) in the degradation of CIPRO was determined using two-way analysis of variance (ANOVA).

3. RESULTS AND DISCUSSION

3.1. Extraction and SDS-PAGE of Sericin. Sericin is a group of glycoproteins with molecular weights ranging from 10 to >400 kDa.[59] The two molecular weight distributions of sericin extracted in the present study were confirmed by SDS-PAGE. On the one hand, GuHCl, a chaotropic agent that disturbs the hydrogen bond of protein to unfold the structure,[60] was used for sericin solubilization for the study at an optimum temperature of 60 °C.[61] The percentage yield obtained was 5.87 ± 0.40%, which is much lower than 25% of all sericin present in silk, indicating that only a part of the sericin was removed in this process. Three distinct bands at 415, 243, and 40 kDa along with some low-molecular-weight bands were observed in lane 1 (Figure 1, lane 1). On the other hand, sodium carbonate (Na_2CO_3), an alkali, is an effective technique to degum silk, but the process degrades sericin significantly.[62,63] This degradation is not a problem in the textile industry since sericin is not used and is disposed of as waste. In this approach, as expected, the yield of sericin obtained was 26.51 ± 0.10%, 5-fold that obtained for GuHCl extraction. A smeared band in the 30−116 kDa range was observed in lane 2 (Figure 1, lane 2), indicating pronounced degradation of isolated sericin. Gimenes et al.[64] reported the molecular weight of sericin extracted using Na_2CO_3 at 120 °C to be <100 kDa. Chirila et al.[62] reported smeared bands near 35 kDa and minor distribution around 200 kDa. The slight difference in the molecular weight obtained could be due to the difference in extraction conditions like temperature and the

https://doi.org/10.1021/acsomega.3c03367
ACS Omega 2024, 9, 15768−15780

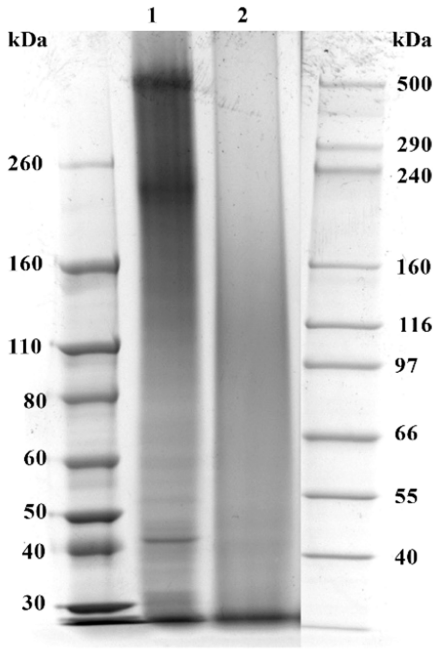

Figure 1. SDS-PAGE of lane 1: high-molecular-weight (HMW) sericin extracted using 6 M GuHCl at 60 °C for 1 h and lane 2: low-molecular-weight (LMW) sericin extracted using boiling 0.02 M Na_2CO_3 for 1 h.

concentration of sodium carbonate. Owing to the difference in the molecular weights of sericin obtained via GuHCl and Na_2CO_3, sericin was termed as high-molecular-weight (HMW) sericin and low-molecular-weight (LMW) sericin, respectively. Both HMW and LMW sericins were studied individually for the formation of nanoflowers and their morphologies and properties.

3.2. Characterization and Peroxidase-Like Activity of Sericin Hybrid Nanoflowers (ShNFs). The coordination between the metal ions and the functional groups of sericin leads to the formation of hybrid nanoflowers, as described by Koley and group.[11,39] Parameters, such as the reactant concentration, incubation temperature and time, and pH of the buffer for synthesis are known to govern the morphology of hybrid nanoflowers, which in turn may alter their physical and chemical properties.[65] The impact of the molecular weight distribution of sericin as a precursor was mostly studied in this work. The concentrations of HMW and LMW sericin were 0.02, 0.04, 0.06, 0.08, and 0.1 mg/mL in PBS while 1.0 mM $CuSO_4{\cdot}5H_2O$ was used. The nanoflowers prepared using HMW and LMW sericin were termed high-molecular-weight sericin hybrid nanoflowers (HMW-ShNFs) and low-molecular-weight sericin hybrid nanoflowers (LMW-ShNFs), respectively.

3.2.1. High-Molecular-Weight Sericin Hybrid Nanoflowers (HMW-ShNFs). The control sample, copper phosphate ($Cu_3(PO_4)_2{\cdot}3H_2O$) precipitate prepared using PBS and $CuSO_4{\cdot}5H_2O$ without sericin, was termed as copper phosphate precipitate (CPP). The average size of CPP was 20.7 ± 1.5 μm (Figure 2A) with a bloomed flower-like morphology and wafer-thin nanopetals. With the addition of 0.02 mg/mL HMW sericin, the size of the nanoflowers increased to 53.5 ± 12.8 μm. As the concentration of HMW sericin increased from 0.02 to 0.1 mg/mL, the morphology of the hybrid nanoflowers was changed, as shown in Figure 2B−F. On increasing the concentration of HMW sericin from 0.02 to 0.04 mg/mL, the HMW sericin loading increased (Figure 2I) and correspondingly the average size of HMW-ShNFs decreased from ∼53.5 ± 12.8 to 43 ± 8.8 μm. Moreover, HMW sericin loading for 0.04 to 0.1 mg/mL appeared to reach saturation with decreasing order of size, with 38 ± 5.2, 19.6 ± 5.1, and 19.7 ± 4.3 μm corresponding to concentrations of 0.06, 0.08, and 0.1 mg/mL of HMW sericin, respectively. This decrease in size could be due to the increased occurrence of nucleation centers, resulting from the increased concentration of binding sites for Cu^{2+} ions as the HMW sericin concentration increased.[23] Also, the petal density gradually increased as a function of protein concentration for values between 0.02 and 0.1 mg/mL.

The impact of varying concentrations of $CuSO_4{\cdot}5H_2O$ (0.6−1 mM) on HMW sericin (0.1 mg/mL) was also investigated. Though HMW-ShNFs were formed, 1.0 mM $CuSO_4{\cdot}5H_2O$ clearly resulted in the formation of complete nanoflower structures. At 0.6 mM $CuSO_4{\cdot}5H_2O$, nanoflowers were found to have many nanosheets agglomerated to form nanopetals with an average size of 61.4 ± 13.3 μm (Figure 2G). With further increase in the $CuSO_4{\cdot}5H_2O$ concentration to 0.8 mM, nanopetals formed were loosely bound in a nanoflower-like structure with an average size of 45.2 ± 11.7 μm (Figure 2H), which was in agreement with a study conducted with modified laccase and Cu^{2+} ions.[66] As the protein-to-metal ion ratio increased from 0.1 mg/mL HMW sericin/0.6 mM Cu^{2+} ions to 0.1 mg/mL HMW sericin/1 mM Cu^{2+} ions, the number of nanocrystals of copper phosphate (nuclei) formed increased, and hence, the size decreased. Therefore, from a purely morphological perspective, the optimal protein-to-metal ion ratio for the formation of nanoflowers was 0.1 mg/mL HMW sericin/1 mM Cu^{2+} ions; a similar finding was reported by Koley et al.[11]

Numerous efforts have been made to develop efficient and cost-effective Cu-based catalysts with peroxidase-mimicking activity. The performance of such catalysts depends on their construction and surface properties. The protein-incorporated nanoflowers possess peroxidase-like activity due to the presence of copper(II).[9] Copper phosphate, a major component of the petals of nanoflowers, along with the protein, exhibits peroxidase-like activity by oxidizing the substrate with free radicals by a Fenton-like mechanism.[67] The reaction between the cupric ions present in the nanoflowers and H_2O_2 resulted in the formation of cuprous ions and peroxide radicals, as shown in Reaction 1 of Scheme 1. Cu^+ ions in turn oxidize H_2O_2 to hydroxyl ($^{\bullet}OH$) radicals (Reaction 2 in Scheme 1). The $^{\bullet}OH$ radicals then oxidize ABTS to its green-colored complex (ABTS radical cation form)[9,40] (Reaction 3 in Scheme 1) that shows an absorbance maximum at 417 nm.[41]

The peroxidase-like activities of CPP and HMW-ShNFs were evaluated in this study. The CPP sample, a control sample prepared without the addition of sericin, exhibited a peroxidase-like activity of 1.3 ± 0.1 U/mL. With the addition of HMW sericin, the peroxidase-like activity of all samples was enhanced (Figure 2J). The peroxidase-like activity increased with an increase in the HMW sericin concentration. This could be related to the smaller size and increased petal density of the respective samples. This may indicate that peroxidase-like activity was generated by CPP, while sericin only helped in the nucleation of CPP in such a manner that the surface area-to-volume ratio increased, thereby increasing the activity of the nanoflowers. Figure 2K shows color development due to

https://doi.org/10.1021/acsomega.3c03367
ACS Omega 2024, 9, 15768−15780

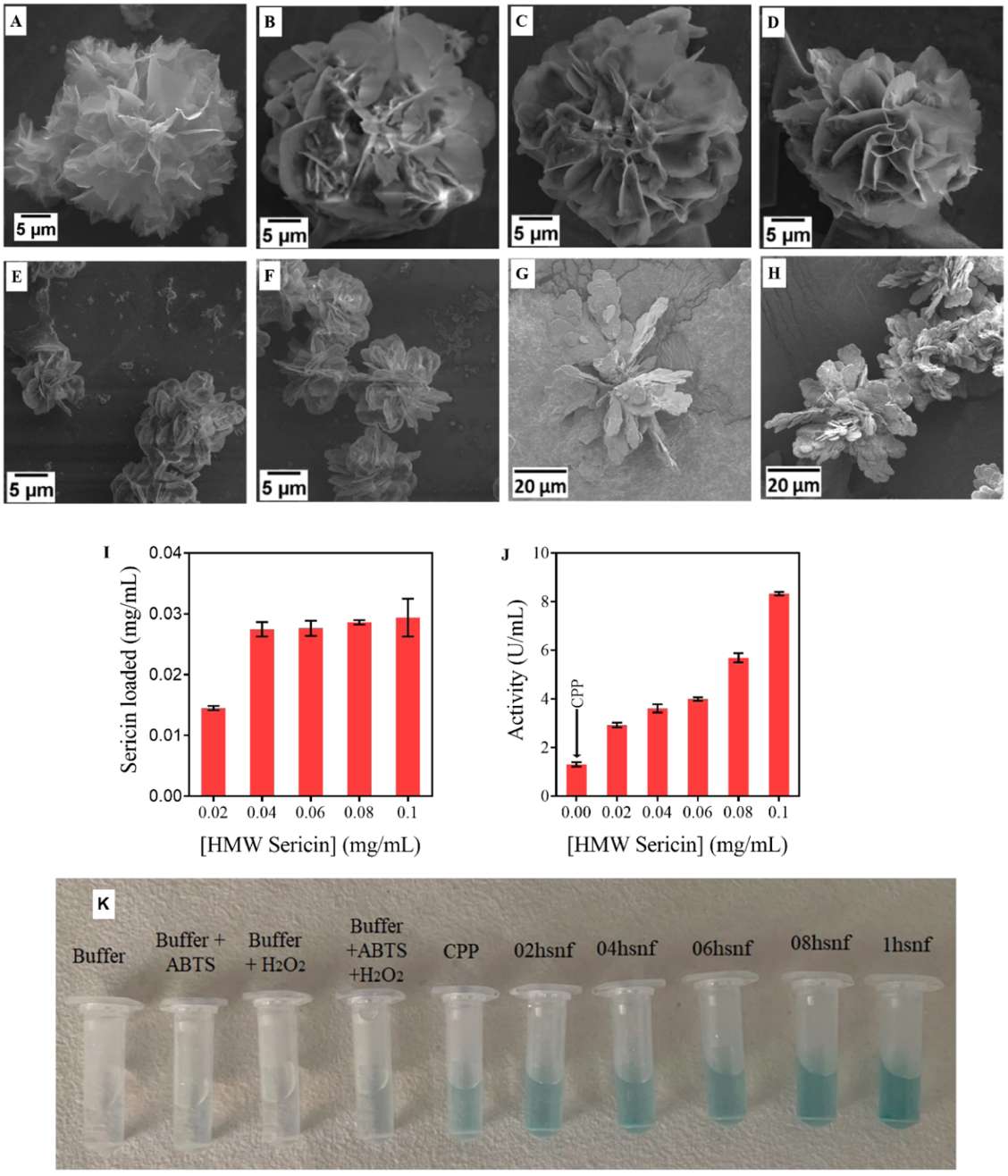

Figure 2. SEM images of (A) copper phosphate precipitate (CPP) prepared without sericin. HMW-ShNFs prepared with varying concentrations of HMW sericin in PBS (10 mM, pH 7.4): (B) 0.02 mg/mL; (C) 0.04 mg/mL; (D) 0.06 mg/mL; (E) 0.08 mg/mL, (F) 0.1 mg/mL with $CuSO_4 \cdot 5H_2O$ (1 mM), (G) 0.1 mg/mL with 0.6 mM $CuSO_4 \cdot 5H_2O$, and (H) 0.1 mg/mL with 0.8 mM $CuSO_4 \cdot 5H_2O$ in PBS (10 mM, pH 7.4) incubated for 72 h undisturbed. (I) HMW sericin loaded with different concentrations of HMW sericin, and (J) peroxidase-like activity of HMW-ShNFs prepared with varying concentrations of sericin. Reaction conditions: $[ABTS]_0$ = 1.5 mM; $[H_2O_2]_0$ = 8 mM; pH_0 = 4.5, with sodium acetate buffer (100 mM) for 10 min at 35 °C. (K) Photographic image of color development under reaction conditions as in (J). Note: The coding of samples is given in Table S1.

peroxidase-like activity of the HMW-ShNFs. To confirm that the activity did not originate from the leaching of copper(II) in the solution, the nanoflowers were suspended in the sodium acetate buffer for 1 h at 35 °C, and then the peroxidase-like activity of the supernatant was determined. No absorbance was observed at 417 nm for the green-colored $ABTS^{\bullet+}$ radical cation, which is in agreement with the study conducted by Huang et al.[13]

3.2.2. Low-Molecular-Weight Sericin Hybrid Nanoflowers (LMW-ShNFs). Unlike the HMW-ShNFs, the LMW-ShNFs were very compact nanoflowers with a large number of agglomerated nanopetals. As the concentration of LMW sericin increased from 0.02 to 0.1 mg/mL, the thickness of the nanopetals increased (Figure 3A–E). However, the size of LMW-ShNFs formed were much smaller ~9.7 ± 1.1, 9.1 ± 0.9, 8.7 ± 0.3, 6.6 ± 0.5, and 5.3 ± 0.4 μm, and were more uniform and monodispersed than HMW-ShNFs. This study was in support of Lei and Zare[23] in that LMW sericin loading increased with an increase in LMW sericin concentration (Figure 3G). The alkaline sericin extraction method had

https://doi.org/10.1021/acsomega.3c03367
ACS Omega 2024, 9, 15768−15780

Scheme 1. Reaction between Cu^{2+}, H_2O_2, and ABTS Exhibiting Peroxidase-Like Activity of ShNFs (Adapted from Wu et al., 2016; "Amino Acids-Incorporated Nanoflowers with an Intrinsic Peroxidase-Like Activity." Published in Scientific Reports; Copyright 2016; Springer Nature; 10.1038/srep22412; under Creative Commons Attribution 4.0 International License; http://creativecommons.org/licenses/by/4.0/)

$$Cu^{2+} + H_2O_2 \rightarrow Cu^{+} + HOO^{\bullet} + H^{+} \quad \text{reaction 1}$$

$$Cu^{+} + H_2O_2 \rightarrow Cu^{2+} + HO^{\bullet} + OH^{-} \quad \text{reaction 2}$$

$$HO^{\bullet} + ABTS \rightarrow ABTS^{\bullet+} + H_2O \quad \text{reaction 3}$$

pronounced degradation effects on sericin, and smaller molecular weight bands were observed. This indicates the availability of two more functional groups due to chain scission, thereby increasing the number of easily accessible chelating groups and, therefore, opportunities for nucleation centers to form, thus resulting in the formation of much smaller-sized nanoflowers. Spherical nanoflowers with a maximum density of nanopetals were observed in this case. This is likely due to the same factors. As the concentration of $CuSO_4{\cdot}5H_2O$ was decreased to 0.6 mM, not much change in the formation of nanopetals was observed (Figure 3F).

Similar to HMW-ShNFs, the use of LMW sericin also increased the peroxidase-like activity of LMW-ShNFs compared to CPP (Figure 3H). The activity as a function of concentration initially increased for protein concentrations between 0.02 and 0.04 mg/mL; however, with further increase of the LMW sericin concentration, the activity started to decrease. Figure 3I shows color development due to the peroxidase-like activity of the LMW-SHNFs. Additionally, the overall peroxidase-like activity of LMW-ShNFs was lower than that of HMW-ShNFs. Even though the surface of the LMW-ShNFs appeared to be porous, thicker nanopetals were formed in the case of the LMW-ShNFs, and LMW sericin residues on the LMW-ShNFs may have restricted the interactions of Cu^{2+} with H_2O_2 and ABTS (diffusion-limiting morphological effect).

A second experiment was carried out to ensure that color development was not the result of Cu^{2+} ion leaching from the nanoflowers. Two Eppendorf tubes with working buffers were obtained, one of which had nanoflowers added, and the other was used as a control. Except for ABTS, both samples were subjected to the same testing procedures used to assess peroxidase-like activity. The nanoflowers were removed after 30 min via centrifugation, and both solutions were subjected to UV−visible analysis. Both UV−visible spectra, as shown in Figure S1, were comparable. Therefore, it was concluded that there was no leaching of Cu^{2+} ions during the analysis.

Overall, the order of activity was as follows: HMW-ShNFs > LMW-ShNFs > CPP. Wang et al.[40] reported peroxidase-like activity of 0.01488 μmol/mg/min for lysine nanoflowers and 0.00457 μmol/mg/min for CPP under similar conditions. This difference could be due to the higher concentrations of HMW-ShNFs and LMW-ShNFs used in the present study. However, horseradish peroxidase (HRP) nanoflowers showed an activity of 17,595 U/mg,[65] which is much higher due to the enzymatic behavior of HRP. Similarly, soybean peroxidase nanoflowers demonstrated activity of 1857 U/mg.[68]

Infrared spectroscopy is an important tool for the determination of the secondary structures of proteins, mainly by analyzing their characteristic amide bands. The characteristic peak at 1631−1650 cm^{-1} corresponds to the amide I group, 1510−1530 cm^{-1} to amide II, and the small peak at 1230−1250 cm^{-1} to the amide III group signifies the presence of sericin in the ShNFs. The peaks at 1030−1050 and 980−995 cm^{-1} (a) confirm the presence of phosphate groups in the ShNFs (Figure S2). This is in agreement with the work conducted by Koley et al.[11] The broad peak at 3440 cm^{-1} for CPP could be attributed to the OH group. However, the slightly broad and sharp peak at 3285 cm^{-1} for the HMW-ShNFs could be attributed to the overlap of the NH and OH groups. On the contrary, the presence of −OH, −NH, and −COOH groups due to the use of a shorter protein chain resulted in a much broader peak at 3266 cm^{-1} for the LMW-ShNFs.

The crystal structures of both HMW-ShNFs and LMW-ShNFs were studied using X-ray diffraction (XRD). The copper phosphate precipitate (CPP) prepared in the absence of the protein molecule was used as a control. In Figure S3, the diffraction angles (i.e., 2θ) of CPP, HMW-ShNFs, and LMW-ShNFs were comparable to those of JPSCD 00-022-0548.

The presence of phosphorus and copper along with carbon and oxygen in the EDX spectra (Figure S4) confirmed the successful synthesis of HMW-ShNFs and LMW-ShNFs. The nickel detected was from the grid used. The presence of chloride could be from the PBS residue.

3.3. Reusability and Stability Tests for ShNFs. Biocatalysts with long-term stability are desirable, as they may contribute to reducing the expenditure for repetitive preparation and reduce the waste of chemicals. The nanoflower samples with the highest peroxidase-like activity from the HMW-ShNF and LMW-ShNF sets were used for conducting reusability and stability tests. Figure 4A shows the reusability of HMW-ShNFs and LMW-ShNFs. With consecutive use, the peroxidase-like activity of both nanoflower samples decreased. By the sixth cycle, ∼55 and ∼65% of the initial activities of the HMW-ShNFs and LMW-ShNFs were retained, respectively. Even though LMW-ShNFs were able to retain a greater percentage of activity during the centrifugation with high centrifugal forces, the residual activity of HMW-ShNFs was still significantly higher than that of LMW-ShNFs. The compact structure of LMW-ShNFs could have reduced the rate of disintegration (or loss) of nanoflowers due to centrifugation compared to HMW-ShNFs.

The nanoflowers stored in PBS (10 mM, pH 7.4) at 4 °C for 30 days were monitored every seventh day for storage stability. Figure 4B presents the stability tests for the HMW-ShNFs and LMW-ShNFs. The rate of decline of peroxidase-like activity for HMW-ShNFs was observed to be very low. The HMW-ShNFs were able to preserve about 86% of their activity until the 29th day. This is in line with the morphological observations by SEM (Figure 4C), where a slight change in the structure of the HMW-ShNFs was observed over the same time frames. On the contrary, the LMW-ShNFs retained only 64% of their activity. This decline in the activity was also in line with the SEM images shown in Figure 4D, where the LMW-ShNFs started to show signs of degradation by the 29th day in PBS at 4 °C. The size of the majority of the LMW-ShNFs decreased significantly.

The activity, reusability, and stability tests of the ShNFs showed that sericin removal, such as Na_2CO_3 degumming for textile applications, prioritizes degumming efficiency (weight loss) without too much loss of fiber strength. However, it causes significant degradation of sericin, which is not a

https://doi.org/10.1021/acsomega.3c03367
ACS Omega 2024, 9, 15768−15780

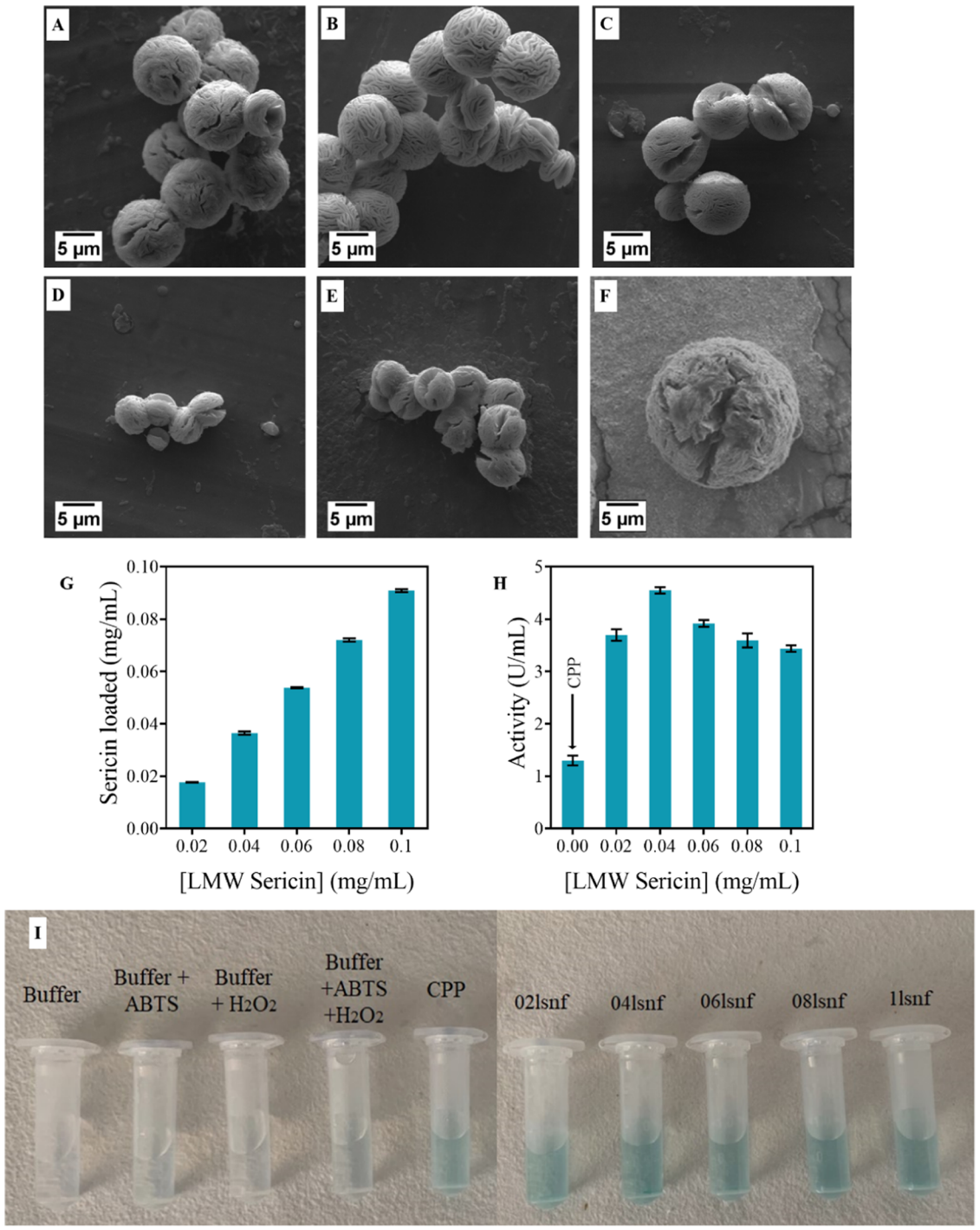

Figure 3. SEM images of LMW-ShNFs prepared with varying concentrations of LMW sericin in PBS (10 mM, pH 7.4): (A) 0.02 mg/mL, (B) 0.04 mg/mL, (C) 0.06 mg/mL, (D) 0.08 mg/mL, (E) 0.1 mg/mL with $CuSO_4{\cdot}5H_2O$ (1 mM), and (F) 0.1 mg/mL of LMW sericin with $CuSO_4{\cdot}5H_2O$ (0.6 mM) and incubated for 72 h undisturbed. (G) LMW sericin loaded at different concentrations of HMW sericin, and (H) peroxidase-like activity of LMW-ShNFs prepared at varying concentrations of sericin. Reaction conditions: $[ABTS]_0$ = 1.5 mM; $[H_2O_2]_0$ = 8 mM; pH_0 = 4.5 with sodium acetate buffer (100 mM) for 10 min at 35 °C. (I) Photographic image of color development under reaction conditions as in (H). Note: the coding of the samples is given in Table S1.

problem for the textile industry but is not an ideal approach when sericin is the desired end product. On the contrary, the GuHCl approach explored in this study extracts sericin with minimal hydrolysis; however, it is not suitable for the textile industry. Although less efficient due to lower extraction yield, the less-degraded sericin that is extracted has significantly different molecular weights and properties compared to alkaline-extracted sericin. The key message, therefore, is the need for more efficient degumming of silk, which can remove sericin efficiently but maintain its molecular weight, if applications of sericin, such as in nanoflowers with peroxidase-like activity, are of interest.

3.4. Kinetic Study of ShNFs. The kinetic parameters of HMW-ShNFs and LMW-ShNFs in the reactions discussed

https://doi.org/10.1021/acsomega.3c03367
ACS Omega 2024, 9, 15768−15780

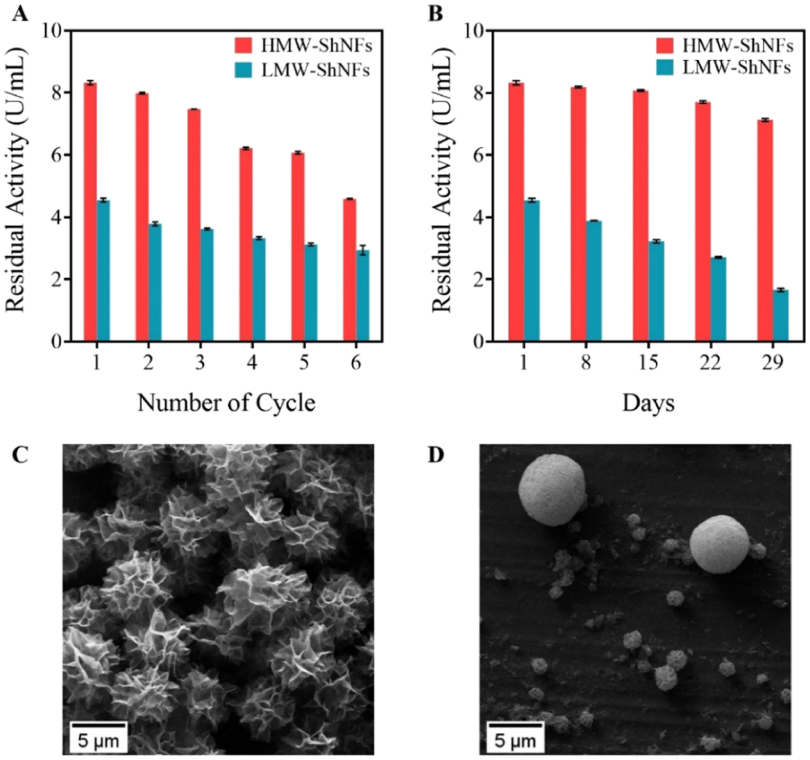

Figure 4. (A) Reusability of HMW-ShNFs (1hsnf) and LMW-ShNFs (04lsnf). (B) Storage stability of HMW-ShNFs (1hsnf) and LMW-ShNFs (04lsnf). Error bars represent standard deviations obtained from triplicate samples. SEM images of (C) HMW-ShNFs after 29 days of storage and (D) LMW-ShNFs after 29 days of storage in PBS (10 mM, pH 7.4) at 4 °C.

were determined by using the Michaelis−Menten model (Figure S5). The peroxidase-like activity of ShNFs was measured by varying the concentration of ABTS as a substrate. The K_m values of HMW-ShNFs and LMW-ShNFs against ABTS were 0.65 ± 0.05 and 5.39 ± 0.93 mM, respectively (Table 1). The variation in the K_m values of the HMW-ShNFs and LMW-ShNFs could be due to the significant difference in the morphologies of the respective nanoflowers. The rosette-like structure of HMW-ShNFs may provide easy access to the active binding site present in the nanoflowers by the substrate and may result in a lower K_m value, whereas LMW-ShNFs form a very compact structure with thicker nanopetals, which could hinder the binding of the substrate to the active site. One of the already reported nanoflowers like hemin−concanavalin A hybrid nanoflowers was reported to have a K_m value of 0.2248 mM at RT against ABTS.[58] The lower value of K_m could be due to the dual protein immobilized in the nanoflowers, thereby showing better affinity to ABTS. On the other hand, the K_m value for BSA hybrid nanoflowers was 35.18 mM against 3,3,5,5-tetramethylbenzidine (TMB);[13] however, this large difference could be due to the different substrates used. A biocatalyst with a small K_m value and a high V_{max} value is generally ideal for catalytic activity. However, the V_{max} of HMW-ShNFs was estimated to be 2.12 μM/min, which is much lower compared to LMW-ShNFs having a V_{max} of 11.23 μM/min. This could be due to the difference in size and morphology of the nanoflowers, as the concentration of nanoflowers used in the study was the same. Due to the much smaller size of the LMW-ShNFs (9.01 ± 0.12 μm), 1 mg of LNW-ShNFs in 1 mL could possibly have a much greater number of nanoflowers in the reaction mixture compared to HMW-ShNFs (19.65 ± 4.25 μm). The presence of a larger number of nanoflowers in the LMW-ShNFs could be the reason for a higher V_{max}.

Table 1. Kinetic Parameters for ShNFs

ShNFs	K_m (mM)	V_{max} (μM/min)
HMW-ShNFs	0.65 ± 0.05	2.12
LMW-ShNFs	5.39 ± 0.93	11.23

Although efforts are being made to prepare hybrid nanoflowers with intrinsic peroxidase activity, the literature on the kinetics of hNF reactions is limited. This study can serve as a starting point for the future development of hybrid nanoflowers with peroxidase-like activity. Moreover, biocatalysts with long-term reusability and stability are desirable, as they can eliminate the need for repetitive preparation and reduce expenditures. Therefore, HMW-ShNFs with higher reusability and stability than LMW-ShNFs were used for the degradation study of ciprofloxacin.

3.5. Peroxidase-Based Degradation of Ciprofloxacin Using HMW-ShNFs. Owing to the activity and stability of ShNFs, HMW-SHNFs were shortlisted for peroxidase-based degradation of ciprofloxacin. pH plays an important role in the degradation of organic pollutants. The degradation of ciprofloxacin was performed at four different pH values: 4.5, 6.5, 8, and 10. In the acidic range (pH 4.5), a very low degradation efficiency of 1.28 ± 0.09% was observed. As the pH increased to neutral (pH 6.5), the degradation efficiency increased to 11.68 ± 0.60%, and on further increasing the pH to 8, a value of 26.52 ± 0.46% for the degradation of ciprofloxacin was obtained (Figure 5A). The Fe^{2+}/H_2O_2 system was previously used as Fenton's reagent for peroxidase activity tests; however, it was effective in the acidic range.

https://doi.org/10.1021/acsomega.3c03367
ACS Omega 2024, 9, 15768−15780

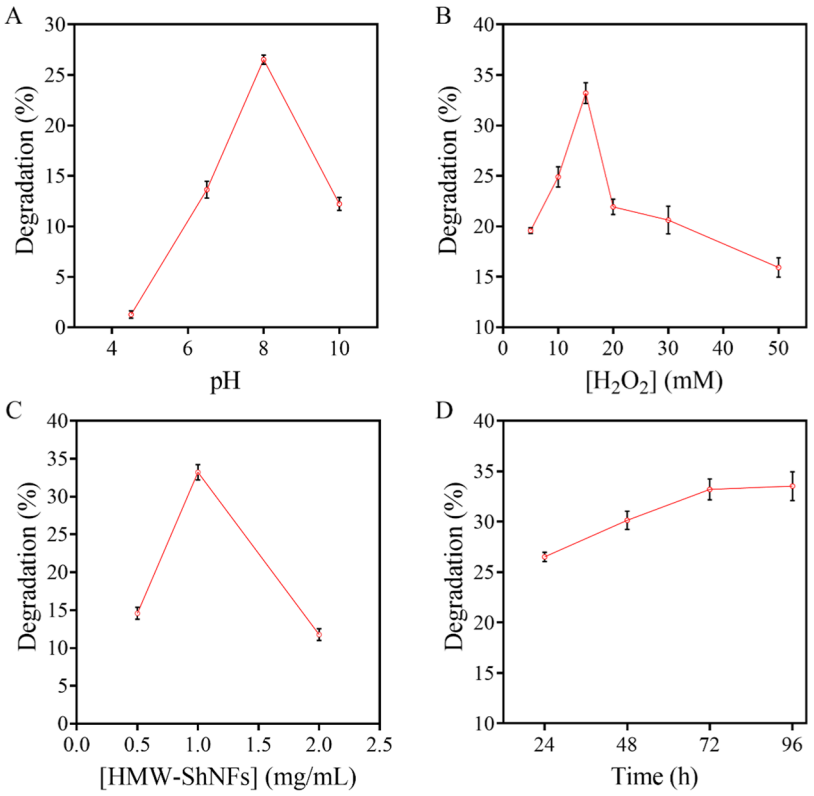

Figure 5. Optimization for peroxidase-based degradation of CIPRO: (A) pH, (B) $[H_2O_2]_0$ = 5−50 mM, (C) $[HMW\text{-}ShNFs]_0$ = 0.5−2.0 mg/mL, and (D) time = 24−96 h. Reaction conditions: $[CIPRO]_0$ = 10 ppm and 35 °C. Error bars represent standard deviations obtained from triplicate samples.

Table 2. Copper-Based Catalysts for the Degradation of CIPRO

catalysts	mediator	pH	catalysts dosage (g/L)	[CIPRO] (ppm)	time	degradation efficiency (%)	remark	references
zero-valent copper nanoparticles	in the presence of oxygen, Cu(I) and H_2O_2 are generated in situ	3.5	1.25	20	120 min	100	formation of active radical species of oxygen	73
nano-zero-valent copper	$[H_2O_2]$ = 40 ppm	8	0.5	10	105 min	85	hydroxyl radicals	71
nanoscale zero-valent copper	ascorbic acid (1 mM)	6.3	0.1	5	60 min	85	formation of superoxide and hydroxyl radicals	74
nano-zero-valent copper-modified biochar		6.5	0.5	10	105	88	removal of CIPRO via hydroxyl radicals and adsorption	75
HMW-ShNFs	$[H_2O_2]$ = 15 mM	8	1	10	24 h	33.2	generation of hydroxyl radicals	present work

Cu^{2+}/H_2O_2 has been reported to produce •OH radicals over a larger pH range than the Fe^{2+}/H_2O_2 system.[69,70] As presented in the previous section for the detection of H_2O_2, •OH radicals formed at pH 4.5 were able to oxidize ABTS to the cationic radical form; however, •OH radicals were inefficient in the breakdown of ciprofloxacin. As the pH moved toward neutral, the degradation efficiency increased. This is probably because ciprofloxacin exists as a zwitterion at pH 6−8, which makes the degradation more efficient. At pH > 9, the degradation efficiency decreased again. The reduction in degradation efficiency at acidic and alkaline conditions could be due to the repulsion between CIPRO and HMW-ShNFs, as they both have identical charges at acidic and alkaline conditions.[71]

Hydrogen peroxide was also found to have a significant influence on the degradation of ciprofloxacin. As the concentration of H_2O_2 increased from 5 to 15 mM, the degradation efficiency increased from 19.54 ± 0.31 to 33.20 ± 1.03% (Figure 5B). This increase was assumed to be due to the increased production of •OH radicals caused by the increase in the concentration of H_2O_2. Upon further increasing the H_2O_2 concentration, a steady decline in the degradation process was noticed. This could be due to the effect of excess H_2O_2 concentration in the solution.[72] Further, the requirement for an optimal amount of biocatalyst plays a crucial role in the degradation studies. The optimal concentration of HMW-ShNFs was found to be 1.0 mg/mL with 33.20 ± 1.03% degradation of ciprofloxacin. Upon either increasing or decreasing the amount of biocatalyst, a decline in the degradation efficiency of CIPRO (Figure 5C) was observed. H_2O_2 alone in the absence of HMW-ShNFs did not show any appreciable ciprofloxacin degradation efficiency, which is in line with some previous works.[71] Therefore, it was also confirmed that the formation of •OH radicals was caused by HMW-ShNFs.

https://doi.org/10.1021/acsomega.3c03367
ACS Omega 2024, 9, 15768−15780

Scheme 2. Proposed Mechanism for Ciprofloxacin Degradation

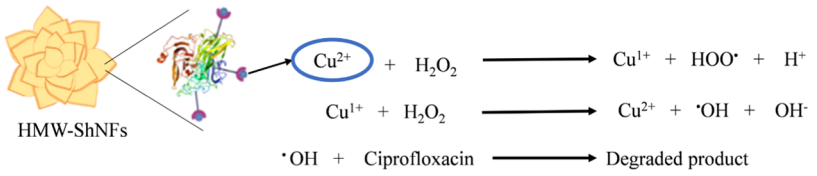

The degradation of ciprofloxacin in optimal conditions, i.e., [HMW-ShNFs] = 1 mg/mL, [H_2O_2] = 15 mM, and pH = 8 was monitored every 24 h until 96 h elapsed. The results indicate that the majority of the degradation (26.52 ± 0.46%) occurred in the initial 24 h. Beyond 24 h, the increase in ciprofloxacin degradation was only ∼3%; hence, the study was not continued after 96 h (Figure 5D). This is the first study to report on the degradation of ciprofloxacin with sericin−copper hybrid nanoflowers. The degradation efficiency of HMW-ShNFs reported in this paper is summarized in Table S3.

As summarized in Table 2, previously reported zero-valent copper-based catalysts exhibited excellent Fenton-like reactions for the degradation of CIPRO due to the formation of reactive oxygen species. However, the present study involved the use of divalent copper, which upon reaction with H_2O_2 only produces hydroxyl radicals; hence, a lower degradation efficiency was observed. Therefore, as discussed in Section 3.2, the reaction between the cupric (Cu^{2+}) ions present in the nanoflowers and H_2O_2 results in the formation of cuprous (Cu^{+}) ions and peroxide radicals. The Cu^{+} ions in turn oxidize H_2O_2 to hydroxyl ($^{\bullet}OH$) radicals, which in turn oxidize ciprofloxacin (Scheme 2).

4. CONCLUSIONS

In conclusion, this article discussed the impact of two different extraction approaches on the morphology and peroxidase-like activity of nanoflowers prepared. The HMW sericin resulted in a bloomed flower-like structure, whereas the LMW sericin resulted in a spherical-shaped closed bud-like structure due to the widely available functional groups on the shorter chains. The Cu^{2+} ions in the nanoflowers were stabilized by the functional groups of sericin while maintaining their catalytic properties in the presence of H_2O_2. ShNFs were successfully able to oxidize ABTS to the $ABTS^{\bullet+}$ radical cations. The HMW-ShNFs and LMW-ShNFs were found to have higher peroxidase-like activity than the CPP ($Cu_3(PO_4)_2{\cdot}3H_2O$ precipitate), demonstrating the importance of sericin as an organic moiety for the preparation of such nanoflowers. Therefore, these ShNFs may be used as biosensors for the detection of H_2O_2 in future work. In comparison to the LMW-ShNFs, the HMW-ShNFs showed superior peroxidase-like activity, reusability, and storage stability. Therefore, HMW-ShNFs were used to study the degradation of ciprofloxacin. The peroxidase-based degradation studies using HMW-ShNFs in the presence of H_2O_2 led to 26.5% degradation of ciprofloxacin in 24 h at pH 8. Overall, the HMW-ShNFs were found to be promising and worthy of further exploration considering their good recyclability and storage stability.

■ ASSOCIATED CONTENT

Supporting Information

The Supporting Information is available free of charge at https://pubs.acs.org/doi/10.1021/acsomega.3c03367.

Coding for variants of HMW-ShNFs and LMW-ShNFs prepared with 1 mM $CuSO_4{\cdot}5H_2O$; UV−vis spectra, FTIR spectra, XRD spectra with diffraction angles, EDX spectra, Michaelis−Menten plot of HMW-ShNFs and LMW-ShNFs; table for peroxidase-based degradation of CIPRO using HMW-ShNFs (PDF)

■ AUTHOR INFORMATION

Corresponding Author

Ruchi Agrawal − *TERI-Deakin Nanobiotechnology Centre, Sustainable Agriculture Division, The Energy and Resources Institute, TERI Gram, Gwal Pahari, Gurugram, Haryana 122001, India;* orcid.org/0000-0003-0168-6000; Email: dr.ruchiagrawal010@gmail.com

Authors

Divya S. Koshy − *TERI-Deakin Nanobiotechnology Centre, Sustainable Agriculture Division, The Energy and Resources Institute, TERI Gram, Gwal Pahari, Gurugram, Haryana 122001, India; Institute for Frontier Materials, Deakin University, Geelong, VIC 3216, Australia;* orcid.org/0000-0001-6522-3326

Benjamin J. Allardyce − *Institute for Frontier Materials, Deakin University, Geelong, VIC 3216, Australia*

Ludovic F. Dumée − *Department of Chemical Engineering, Khalifa University of Science and Technology, Abu Dhabi 127788, UAE;* orcid.org/0000-0002-0264-4024

Alessandra Sutti − *Institute for Frontier Materials, Deakin University, Geelong, VIC 3216, Australia*

Rangam Rajkhowa − *Institute for Frontier Materials, Deakin University, Geelong, VIC 3216, Australia*

Complete contact information is available at: https://pubs.acs.org/10.1021/acsomega.3c03367

Notes

The authors declare no competing financial interest.

■ ACKNOWLEDGMENTS

The authors are thankful to Deakin University, Geelong, Australia, for providing all infrastructural, analytical, and financial support as an incubation center at TERI-Deakin Nanobiotechnology Center (TDNBC), TERI, India. All the financial, adminstrative, and infrastructural support provided by the TERI is duly acknowledged. The SERB (Science and Engineering Research Board) and DBT (Department of Biotechnology), Ministry of Science and Technology, Govt. of India, are duly acknowledged for providing the funding and other economic assistance. This work was supported in part by Deakin University and, in part, by the Australian Research Council grants number ARC IH140100018 and ARC IH21010002.

https://doi.org/10.1021/acsomega.3c03367
ACS Omega 2024, 9, 15768−15780

ABBREVIATIONS

hNFs - hybrid nanoflowers; ShNFs - sericin hybrid nanoflowers; LMW-ShNFs - low-molecular-weight sericin hybrid nanoflowers; HMW-ShNFs - high-molecular-weight sericin hybrid nanoflowers; ABTS - 2,2′-azino-bis(3-ethylbenzothiazoline-6-sulfonic acid)

REFERENCES

(1) Lu, X.; Li, Y.; Zhang, X.; Du, J.; Zhou, X.; Xue, Z.; Liu, X. A simple and an efficient strategy to synthesize multi-component nanocomposites for biosensor applications. *Anal. Chim. Acta* **2012**, *711*, 40−45.

(2) Zhu, L.; Gong, L.; Zhang, Y.; Wang, R.; Ge, J.; Liu, Z.; Zare, R. N. Rapid Detection of Phenol Using a Membrane Containing Laccase Nanoflowers. *Chem. - Asian J.* **2013**, *8* (10), 2358−2360.

(3) Lin, Z.; Xiao, Y.; Yin, Y.; Hu, W.; Liu, W.; Yang, H. Facile Synthesis of Enzyme-Inorganic Hybrid Nanoflowers and Its Application as a Colorimetric Platform for Visual Detection of Hydrogen Peroxide and Phenol. *ACS Appl. Mater. Interfaces* **2014**, *6* (13), 10775−10782.

(4) Cao, H.; Yang, D.-P.; Ye, D.; Zhang, X.; Fang, X.; Zhang, S.; Liu, B.; Kong, J. Protein-inorganic hybrid nanoflowers as ultrasensitive electrochemical cytosensing Interfaces for evaluation of cell surface sialic acid. *Biosens. Bioelectron.* **2015**, *68*, 329−335.

(5) Lu, C.; Liu, X.; Li, Y.; Yu, F.; Tang, L.; Hu, Y.; Ying, Y. Multifunctional janus hematite−silica nanoparticles: mimicking peroxidase-like activity and sensitive colorimetric detection of glucose. *ACS Appl. Mater. Interfaces* **2015**, *7* (28), 15395−15402.

(6) Ariza-Avidad, M.; Salinas-Castillo, A.; Capitán-Vallvey, L. A 3D μPAD based on a multi-enzyme organic−inorganic hybrid nanoflower reactor. *Biosens. Bioelectron.* **2016**, *77*, 51−55.

(7) Sun, J.; Ge, J.; Liu, W.; Lan, M.; Zhang, H.; Wang, P.; Wang, Y.; Niu, Z. Multi-enzyme co-embedded organic−inorganic hybrid nanoflowers: synthesis and application as a colorimetric sensor. *Nanoscale* **2014**, *6* (1), 255−262.

(8) Altinkaynak, C.; Yilmaz, I.; Koksal, Z.; Özdemir, H.; Ocsoy, I.; Özdemir, N. Preparation of lactoperoxidase incorporated hybrid nanoflower and its excellent activity and stability. *Int. J. Biol. Macromol.* **2016**, *84*, 402−409.

(9) Batule, B. S.; Park, K. S.; Gautam, S.; Cheon, H. J.; Kim, M. I.; Park, H. G. Intrinsic peroxidase-like activity of sonochemically synthesized protein copper nanoflowers and its application for the sensitive detection of glucose. *Sens. Actuators, B* **2019**, *283*, 749−754.

(10) Hu, R.; Zhang, X.; Zhao, Z.; Zhu, G.; Chen, T.; Fu, T.; Tan, W. DNA nanoflowers for multiplexed cellular imaging and traceable targeted drug delivery. *Angew. Chem.* **2014**, *126* (23), 5931−5936.

(11) Koley, P.; Sakurai, M.; Aono, M. Controlled Fabrication of Silk Protein Sericin Mediated Hierarchical Hybrid Flowers and Their Excellent Adsorption Capability of Heavy Metal Ions of Pb(II), Cd(II) and Hg(II). *ACS Appl. Mater. Interfaces* **2016**, *8* (3), 2380−2392.

(12) Lin, Z.; Xiao, Y.; Wang, L.; Yin, Y.; Zheng, J.; Yang, H.; Chen, G. Facile synthesis of enzyme−inorganic hybrid nanoflowers and their application as an immobilized trypsin reactor for highly efficient protein digestion. *RSC Adv.* **2014**, *4* (27), 13888−13891.

(13) Huang, Y.; Ran, X.; Lin, Y.; Ren, J.; Qu, X. Self-assembly of an organic−inorganic hybrid nanoflower as an efficient biomimetic catalyst for self-activated tandem reactions. *Chem. Commun.* **2015**, *51* (21), 4386−4389.

(14) He, X.; Chen, L.; He, Q.; Xiao, H.; Zhou, X.; Ji, H. Cytochrome P450 Enzyme-Copper Phosphate Hybrid Nano-Flowers with Superior Catalytic Performances for Selective Oxidation of Sulfides. *Chin. J. Chem.* **2017**, *35* (5), 693−698.

(15) Wu, Z.; Li, H.; Zhu, X.; Li, S.; Wang, Z.; Wang, L.; Li, Z.; Chen, G. Using Laccases in the Nanoflower to Synthesize Viniferin. *Catalysts* **2017**, *7* (6), 188.

(16) Altinkaynak, C.; Kocazorbaz, E.; Özdemir, N.; Zihnioglu, F. Egg white hybrid nanoflower (EW-hNF) with biomimetic polyphenol oxidase reactivity: synthesis, characterization and potential use in decolorization of synthetic dyes. *Int. J. Biol. Macromol.* **2018**, *109*, 205−211.

(17) Jiao, J.; Xin, X.; Wang, X.; Xie, Z.; Xia, C.; Pan, W. Self-assembly of biosurfactant−inorganic hybrid nanoflowers as efficient catalysts for degradation of cationic dyes. *RSC Adv.* **2017**, *7* (69), 43474−43482.

(18) Li, H.; Hou, J.; Duan, L.; Ji, C.; Zhang, Y.; Chen, V. Graphene oxide-enzyme hybrid nanoflowers for efficient water soluble dye removal. *J. Hazard. Mater.* **2017**, *338*, 93−101.

(19) Rong, J.; Zhang, T.; Qiu, F.; Zhu, Y. Preparation of Efficient, Stable, and Reusable Laccase−Cu3(PO4)2 Hybrid Microspheres Based on Copper Foil for Decoloration of Congo Red. *ACS Sustainable Chem. Eng.* **2017**, *5* (5), 4468−4477.

(20) Patel, S. K.; Otari, S. V.; Li, J.; Kim, D. R.; Kim, S. C.; Cho, B.-K.; Kalia, V. C.; Kang, Y. C.; Lee, J.-K. Synthesis of cross-linked protein-metal hybrid nanoflowers and its application in repeated batch decolorization of synthetic dyes. *J. Hazard. Mater.* **2018**, *347*, 442−450.

(21) Sondhi, S.; Kaur, R.; Kaur, S.; Kaur, P. S. Immobilization of laccase-ABTS system for the development of a continuous flow packed bed bioreactor for decolorization of textile effluent. *Int. J. Biol. Macromol.* **2018**, *117*, 1093−1100.

(22) Fu, M.; Xing, J.; Ge, Z. Preparation of laccase-loaded magnetic nanoflowers and their recycling for efficient degradation of bisphenol A. *Sci. Total Environ.* **2019**, *651*, 2857−2865.

(23) Ge, J.; Lei, J.; Zare, R. N. Protein−inorganic hybrid nanoflowers. *Nat. Nanotechnol.* **2012**, *7*, 428.

(24) Koshy, D. S.; Das, R. K. Studies on the role of curcumin concentration, synthesis time, mechanism of formation, and fluorescence properties of curcumin−copper phosphate hybrid nanoflowers. *Inorg. Nano-Met. Chem.* **2021**, *51*, 1499−1506.

(25) Baldemir, A.; Köse, N. B.; Ildız, N.; İlgün, S.; Yusufbeyoğlu, S.; Yilmaz, V.; Ocsoy, I. Synthesis and characterization of green tea (Camellia sinensis (L.) Kuntze) extract and its major components-based nanoflowers: a new strategy to enhance antimicrobial activity. *RSC Adv.* **2017**, *7* (70), 44303−44308.

(26) Zhu, X.; Huang, J.; Liu, J.; Zhang, H.; Jiang, J.; Yu, R. A dual enzyme-inorganic hybrid nanoflower incorporated microfluidic paper-based analytic device (muPAD) biosensor for sensitive visualized detection of glucose. *Nanoscale* **2017**, *9* (17), 5658−5663.

(27) Guo, J.; Wang, Y.; Zhao, M. A self-activated nanobiocatalytic cascade system based on an enzyme-inorganic hybrid nanoflower for colorimetric and visual detection of glucose in human serum. *Sens. Actuators, B* **2019**, *284*, 45−54.

(28) Sharma, N.; Parhizkar, M.; Cong, W.; Mateti, S.; Kirkland, M. A.; Puri, M.; Sutti, A. Metal ion type significantly affects the morphology but not the activity of lipase−metal−phosphate nanoflowers. *RSC Adv.* **2017**, *7* (41), 25437−25443.

(29) Ge, J.; Lei, J.; Zare, R. N. Protein−inorganic hybrid nanoflowers. *Nat. Nanotechnol.* **2012**, *7* (7), 428.

(30) Altinkaynak, C.; Tavlasoglu, S.; Ozdemir, N.; Ocsoy, I. A new generation approach in enzyme immobilization: Organic-inorganic hybrid nanoflowers with enhanced catalytic activity and stability. *Enzyme Microb. Technol.* **2016**, *93*−*94*, 105−112.

(31) Gao, J.; Liu, H.; Pang, L.; Guo, K.; Li, J. Biocatalyst and Colorimetric/Fluorescent Dual Biosensors of H_2O_2 Constructed via Hemoglobin−Cu3(PO4)2 Organic/Inorganic Hybrid Nanoflowers. *ACS Appl. Mater. Interfaces* **2018**, *10* (36), 30441−30450.

(32) Ye, R.; Zhu, C.; Song, Y.; Lu, Q.; Ge, X.; Yang, X.; Zhu, M. J.; Du, D.; Li, H.; Lin, Y. Bioinspired synthesis of all-in-one organic−inorganic hybrid nanoflowers combined with a handheld pH meter for on-site detection of food pathogen. *Small* **2016**, *12* (23), 3094−3100.

(33) Zhang, Y. Q. Applications of natural silk protein sericin in biomaterials. *Biotechnol. Adv.* **2002**, *20* (2), 91−100.

(34) Altman, G. H.; Diaz, F.; Jakuba, C.; Calabro, T.; Horan, R. L.; Chen, J.; Lu, H.; Richmond, J.; Kaplan, D. L. Silk-based biomaterials. *Biomaterials* **2003**, *24* (3), 401−416.

https://doi.org/10.1021/acsomega.3c03367
ACS Omega 2024, 9, 15768−15780

(35) Kundu, B.; Rajkhowa, R.; Kundu, S. C.; Wang, X. Silk fibroin biomaterials for tissue regenerations. *Adv. Drug Delivery Rev.* **2013**, *65* (4), 457−470.
(36) Aramwit, P.; Siritientong, T.; Srichana, T. Potential applications of silk sericin, a natural protein from textile industry by-products. *Waste Manage. Res.* **2012**, *30* (3), 217−24.
(37) Fan, J. B.; Wu, L. P.; Chen, L. S.; Mao, X. Y.; Ren, F. Z. Antioxidant activities of silk sericin from silkworm Bombyx mori. *J. Food Biochem.* **2009**, *33* (1), 74−88.
(38) Khosa, M. A.; Shah, S. S.; Feng, X. J. Thermodynamic functions of metal−sericin complexation in ultrafiltration study. *J. Membr. Sci.* **2014**, *470*, 1−8.
(39) Koley, P.; Sakurai, M.; Takei, T.; Aono, M. Facile fabrication of silk protein sericin-mediated hierarchical hydroxyapatite-based biohybrid architectures: excellent adsorption of toxic heavy metals and hazardous dye from wastewater. *RSC Adv.* **2016**, *6* (89), 86607−86616.
(40) Wu, Z.-F.; Wang, Z.; Zhang, Y.; Ma, Y.-L.; He, C.-Y.; Li, H.; Chen, L.; Huo, Q.-S.; Wang, L.; Li, Z.-Q. Amino acids-incorporated nanoflowers with an intrinsic peroxidase-like activity. *Sci. Rep.* **2016**, *6*, No. 22412.
(41) Celik, C.; Ildiz, N.; Ocsoy, I. Building block and rapid synthesis of catecholamines-inorganic nanoflowers with their peroxidase-mimicking and antimicrobial activities. *Sci. Rep.* **2020**, *10* (1), No. 2903.
(42) Thawari, A. G.; Rao, C. P. Peroxidase-like Catalytic Activity of Copper-Mediated Protein−Inorganic Hybrid Nanoflowers and Nanofibers of β-Lactoglobulin and α-Lactalbumin: Synthesis, Spectral Characterization, Microscopic Features, and Catalytic Activity. *ACS Appl. Mater. Interfaces* **2016**, *8* (16), 10392−10402.
(43) Fent, K.; Weston, A. A.; Caminada, D. Ecotoxicology of human pharmaceuticals. *Aquat. Toxicol.* **2006**, *76* (2), 122−159.
(44) Larsson, D. G. J.; de Pedro, C.; Paxeus, N. Effluent from drug manufactures contains extremely high levels of pharmaceuticals. *J. Hazard. Mater.* **2007**, *148* (3), 751−755.
(45) Balakrishna, K.; Rath, A.; Praveenkumarreddy, Y.; Guruge, K. S.; Subedi, B. A review of the occurrence of pharmaceuticals and personal care products in Indian water bodies. *Ecotoxicol. Environ. Saf.* **2017**, *137*, 113−120.
(46) Sengar, A.; Vijayanandan, A. Human health and ecological risk assessment of 98 pharmaceuticals and personal care products (PPCPs) detected in Indian surface and wastewaters. *Sci. Total Environ.* **2022**, *807*, No. 150677.
(47) Shehu Imam, S.; Adnan, R.; Mohd Kaus, N. H. Photocatalytic degradation of ciprofloxacin in aqueous media: a short review. *Toxicol. Environ. Chem.* **2018**, *100* (5−7), 518−539.
(48) Sodhi, K. K.; Singh, D. K. Insight into the fluoroquinolone resistance, sources, ecotoxicity, and degradation with special emphasis on ciprofloxacin. *J. Water Process Eng.* **2021**, *43*, No. 102218.
(49) Al-Buriahi, A. K.; Al-shaibani, M. M.; Mohamed, R. M. S. R.; Al-Gheethi, A. A.; Sharma, A.; Ismail, N. Ciprofloxacin removal from non-clinical environment: A critical review of current methods and future trend prospects. *J. Water Process Eng.* **2022**, *47*, No. 102725.
(50) Singh, S. K.; Khajuria, R.; Kaur, L. Biodegradation of ciprofloxacin by white rot fungus Pleurotus ostreatus. *3 Biotech* **2017**, *7* (1), No. 69.
(51) Pan, L.-j.; Li, J.; Li, C.-x.; Tang, X.-d.; Yu, G.-w.; Wang, Y. Study of ciprofloxacin biodegradation by a Thermus sp. isolated from pharmaceutical sludge. *J. Hazard. Mater.* **2018**, *343*, 59−67.
(52) Zhou, Y.; You, S.; Zhang, J.; Wu, M.; Yan, X.; Zhang, C.; Liu, Y.; Qi, W.; Su, R.; He, Z. Copper ions binding regulation for the high-efficiency biodegradation of ciprofloxacin and tetracycline-HCl by low-cost permeabilized-cells. *Bioresour. Technol.* **2022**, *344*, No. 126297.
(53) Yun, H.; Oh, H.; Kim, M. K.; Kwak, H. W.; Lee, J. Y.; Um, I. C.; Vootla, S. K.; Lee, K. H. Extraction conditions of Antheraea mylitta sericin with high yields and minimum molecular weight degradation. *Int. J. Biol. Macromol.* **2013**, *52*, 59−65.
(54) Khire, T. S.; Kundu, J.; Kundu, S. C.; Yadavalli, V. K. The fractal self-assembly of the silk protein sericin. *Soft Matter* **2010**, *6* (9), 2066−2071.
(55) Laemmli, U. K. Cleavage of structural proteins during the assembly of the head of bacteriophage T4. *Nature* **1970**, *227* (5259), 680−685.
(56) Gulmez, C.; Altinkaynak, C.; Ozturkler, M.; Ozdemir, N.; Atakisi, O. Evaluating the activity and stability of sonochemically produced hemoglobin-copper hybrid nanoflowers against some metallic ions, organic solvents, and inhibitors. *J. Biosci. Bioeng.* **2021**, *132* (4), 327−336.
(57) Maurya, S. S.; Nadar, S. S.; Rathod, V. K. Dual activity of laccase-lysine hybrid organic−inorganic nanoflowers for dye decolorization. *Environ. Technol. Innovation* **2020**, *19*, No. 100798.
(58) Wang, K.-Y.; Bu, S.-J.; Ju, C.-J.; Li, C.-T.; Li, Z.-Y.; Han, Y.; Ma, C.-Y.; Wang, C.-Y.; Hao, Z.; Liu, W.-S.; Wan, J.-Y. Hemin-incorporated nanoflowers as enzyme mimics for colorimetric detection of foodborne pathogenic bacteria. *Bioorg. Med. Chem. Lett.* **2018**, *28* (23), 3802−3807.
(59) Takasu, Y.; Yamada, H.; Tsubouchi, K. Isolation of Three Main Sericin Components from the Cocoon of the Silkworm, Bombyx mori. *Biosci., Biotechnol., Biochem.* **2002**, *66* (12), 2715−2718.
(60) Zhu, X.; Wang, D.; Sun, X. S. Physico-chemical properties of camelina protein altered by sodium bisulfite and guanidine-HCl. *Ind. Crops Prod.* **2016**, *83*, 453−461.
(61) Poulsen, J. W.; Madsen, C. T.; Young, C.; Poulsen, F. M.; Nielsen, M. L. Using Guanidine-Hydrochloride for Fast and Efficient Protein Digestion and Single-step Affinity-purification Mass Spectrometry. *J. Proteome Res.* **2013**, *12* (2), 1020−1030.
(62) Chirila, T. V.; Suzuki, S.; McKirdy, N. C. Further development of silk sericin as a biomaterial: comparative investigation of the procedures for its isolation from Bombyx mori silk cocoons. *Prog. Biomater.* **2016**, *5* (2), 135−145.
(63) Wang, W.; Pan, Y.; Gong, K.; Zhou, Q.; Zhang, T.; Li, Q. A comparative study of ultrasonic degumming of silk sericin using citric acid, sodium carbonate and papain. *Color. Technol.* **2019**, *135* (3), 195−201.
(64) Gimenes, M. L.; Silva, V. R.; Vieira, M. G.; Silva, M. G.; Scheer, A. P. High molecular sericin from Bombyx mori cocoons: extraction and recovering by ultrafiltration. *Int. J. Chem. Eng. Appl.* **2014**, *5* (3), 266.
(65) Somturk, B.; Hancer, M.; Ocsoy, I.; Özdemir, N. Synthesis of copper ion incorporated horseradish peroxidase-based hybrid nanoflowers for enhanced catalytic activity and stability. *Dalton Trans.* **2015**, *44* (31), 13845−13852.
(66) Zhu, P.; Wang, Y.; Li, G.; Liu, K.; Liu, Y.; He, J.; Lei, J. Preparation and application of a chemically modified laccase and copper phosphate hybrid flower-like biocatalyst. *Biochem. Eng. J.* **2019**, *144*, 235−243.
(67) Koca, F. D.; Demirezen Yilmaz, D.; Ertas Onmaz, N.; Yilmaz, E.; Ocsoy, I. Green synthesis of allicin based hybrid nanoflowers with evaluation of their catalytic and antimicrobial activities. *Biotechnol. Lett.* **2020**, *42* (9), 1683−1690.
(68) Yu, Y.; Fei, X.; Tian, J.; Xu, L.; Wang, X.; Wang, Y. Self-assembled enzyme−inorganic hybrid nanoflowers and their application to enzyme purification. *Colloids Surf., B* **2015**, *130*, 299−304.
(69) Wang, Q.; Ma, Y.; Xing, S. Comparative study of Cu-based bimetallic oxides for Fenton-like degradation of organic pollutants. *Chemosphere* **2018**, *203*, 450−456.
(70) Chen, T.; Zhu, Z.; Zhang, H.; Shen, X.; Qiu, Y.; Yin, D. Enhanced Removal of Veterinary Antibiotic Florfenicol by a Cu-Based Fenton-like Catalyst with Wide pH Adaptability and High Efficiency. *ACS Omega* **2019**, *4* (1), 1982−1994.
(71) Shah, N. S.; Khan, J. A.; Sayed, M.; Iqbal, J.; Khan, Z. U. H.; Muhammad, N.; Polychronopoulou, K.; Hussain, S.; Imran, M.; Murtaza, B.; Usman, M.; Ismail, I.; Shafique, A.; Howari, F.; Nazzal, Y. Nano-zerovalent copper as a Fenton-like catalyst for the degradation of ciprofloxacin in aqueous solution. *J. Water Process Eng.* **2020**, *37*, No. 101325.

https://doi.org/10.1021/acsomega.3c03367
ACS Omega 2024, 9, 15768−15780

(72) Luo, K.; Yang, Q.; Pang, Y.; Wang, D.; Li, X.; Lei, M.; Huang, Q. Unveiling the mechanism of biochar-activated hydrogen peroxide on the degradation of ciprofloxacin. *Chem. Eng. J.* **2019**, *374*, 520−530.
(73) Sousa, P. V. F. d.; Oliveira, A. F. d.; Silva, A. A. d.; Vaz, B. G.; Lopes, R. P. Study of ciprofloxacin degradation by zero-valent copper nanoparticles. *Chem. Pap.* **2019**, *73* (1), 249−260.
(74) Zhang, K.; Deng, J.; Chen, Y.; Xu, C.; Ye, C.; Ling, X.; Li, X. Ascorbic acid enhanced ciprofloxacin degradation with nanoscale zero-valent copper activated molecular oxygen. *Chemosphere* **2021**, *278*, No. 130354.
(75) Iqbal, J.; Shah, N. S.; Sayed, M.; Khan, J. A.; Imran, M.; Khan, Z. U. H.; Niazi, N. K.; Al-Taani, A. A.; Howari, F.; Nazzal, Y. Exploring the potential of nano-zerovalent copper modified biochar for the removal of ciprofloxacin from water. *Environ. Nanotechnol., Monit. Manage.* **2021**, *16*, No. 100604.

https://doi.org/10.1021/acsomega.3c03367
ACS Omega 2024, 9, 15768−15780